Apoptosis in plants: from semantic appeal to empirical rejection

Elena A. Minina[1,2], Adrian N. Dauphinee[1], Florentine Ballhaus[1], Vladimir Gogvadze[3,4], Andrei P. Smertenko[5] and Peter V. Bozhkov[1]

[1]Department of Molecular Sciences, Uppsala BioCenter, Swedish University of Agricultural Sciences and Linnean Center for Plant Biology, P.O. Box 7015, Uppsala, SE-750 07, Sweden

[2]COS, Heidelberg University. Im Neuenheimer Feld 230. 69120 Heidelberg, Germany

[3]Institute of Environmental Medicine, Division of Toxicology, Karolinska Institutet, Box 210, Stockholm, SE-171 77, Sweden.

[4]Faculty of Medicine, MV Lomonosov Moscow State, University, 119991 Moscow, Russia

[5]Institute of Biological Chemistry, College of Human, Agricultural, and Natural Resource Sciences, Washington State University, Pullman, WA 99164, USA.

Correspondence to Elena A. Minina (alena.minina@slu.se) or Peter V. Bozhkov (peter.bozhkov@slu.se)

* E. A. Minina and A. N. Dauphinee contributed equally to this paper.

Abstract

Animals and plants diverged over one billion years ago and evolved unique mechanisms for many cellular processes, including cell death. Plants lack key instruments of apoptotic cell death, including caspases, Bcl-2 family proteins, and phagocytosis. This casts serious doubts on the occurrence of apoptosis in these organisms. Nevertheless, the concept of plant apoptosis or "apoptotic-like programmed cell death" ("AL-PCD") is wide-spread, primarily due to superficial resemblance between protoplast shrinkage in plant cells dying in response to stress and apoptotic volume decrease preceding animal cell fragmentation into apoptotic bodies. Here, we provide a comprehensive spatio-temporal analysis of cytological and biochemical events occurring during plant cell death previously classified as "AL-PCD". We show that under "AL-PCD" inducing conditions, protoplast shrinkage does not proceed to membrane blebbing and formation of apoptotic bodies. Instead, it coincides with instant ATP depletion and irreversible loss of plasma membrane integrity. Furthermore, neither uncoupling of mitochondria nor Ca^{2+} chelation can prevent protoplast shrinkage and cell death, pointing to passive, energy-independent cell collapse perfectly matching definition of necrosis. Although one cannot exclude the possibility that the very early steps of this cell death are genetically regulated, classifying it as apoptosis or "AL-PCD" is misconception. Our study invalidates the notion that apoptosis is conserved across animal and plant kingdoms and demonstrates the importance of focusing on plant-specific aspects of cell death pathway.

Keywords: apoptosis, apoptotic-like programmed cell death, ferroptosis, heat shock, mitochondrial dysfunction, necrosis, plant cells, plasma membrane integrity, protoplast shrinkage.

Introduction

Programmed cell death (PCD) is a process of cellular suicide aimed at maintaining proper development by counteracting cell proliferation and removing aged cells (Jacobson et al., 1997). PCD also plays an essential role in morphogenesis by eliminating surplus cells and shaping new structures (Suzanne and Steller, 2013; Daneva et al., 2016; Huysmans et al., 2017). Furthermore, stress-triggered PCD restricts the spread of pathogens through tissues and confines damage caused by abiotic factors (Coll et al., 2011; Huysmans et al., 2017; Jorgensen et al., 2017).

In their seminal work published almost half a century ago, Kerr and colleagues (Kerr et al., 1972) named the newly described type of PCD in animals after the process of “falling off” of flower petals or leaves, apoptosis (ancient Greek ἀπόπτωσις, apóptōsis, "falling off"). Since then the apoptotic cell death in animals became one of the most studied pathways (for review see Letai, 2017), while our understanding of plant PCD remains fragmented.

The utmost importance of PCD for all multicellular organisms gave weight to the hypothesis that this process should be evolutionary conserved. Indeed, PCD in animals and plants share quite a number of general similarities attributed to the common features of all eukaryotic cells, e.g. dependency on ATP and protein synthesis, regulated proteolysis, and control over toxicity of the dying cell to its neighbours (Kroemer et al., 2005; van Doorn et al., 2011). On the other hand, differences in plant and animal cell morphology, motility, genome maintenance, trophic strategies and body plan plasticity (Murat et al., 2012; Drost et al., 2017) create very different sets of challenges for development, homeostasis and adaptation to the environment, powering diversification of cell death mechanisms (Bozhkov and Lam, 2011).

After the discovery of apoptosis, numerous non-apoptotic types of PCD were described in animals (Galluzzi et al., 2015, 2018), such as paraptosis (Sperandio et al., 2000), necroptosis (Molnár et al., 2019), ferroptosis (Dixon and Stockwell, 2019), pyroptosis (Miao et al., 2010), and others. Since animals possess multiple PCD pathways, each optimized for a specific physiological requirement, there is no reason to assume that plant evolution did not shape plant-specific PCD mechanisms.

A strong evidence for the existence of plant-specific PCD mechanisms is the lack of plant orthologues for the core apoptotic regulators: caspases and Bcl-2 family proteins (Ameisen, 2002). The closest plant orthologues of caspases, metacaspases, have a different substrate specificity and regulatory features (Minina et al., 2020). It is not yet fully explored what subset of proteases is responsible for caspase-like activity detected during plant PCD (for review see Salvesen et al., 2016). Bcl-2 family proteins play either pro- or anti-apoptotic functions in animals by regulating release of cytochrome *c* from mitochondria (Edlich, 2018). Interestingly, ectopic expression of genes encoding pro- or anti-apoptotic Bcl-2 family members in plants can trigger cell death or reduce its frequency, respectively (Lacomme and Santa Cruz, 1999; Mitsuhara et al., 1999), suggesting potential conservation of the cytochrome *c* release function in animal and plant cell deaths. However, the lack of Bcl-2 genes in plant genomes clearly indicates that although cytochrome *c* release might contribute to plant PCD under certain conditions, it is regulated differently from the apoptotic pathway (Yu et al., 2002; Martínez-Fábregas et al., 2013). Nevertheless, original research and reviews on apoptotic features in plants PCD are still being published (for recent reviews, see Dickman et al., 2017; Kabbage et al., 2017; Valandro et al., 2020) propagating controversial conclusions that require careful consideration.

Apoptotic cell death has typical hallmarks: (i) it is an active, ATP- and caspase-dependent process (Tsujimoto, 1997; Hengartner, 2000); (ii) the plasma membrane (PM) integrity is retained throughout the cell death process and phosphatidylserine is exposed on the outer membrane surface as an “eat-me” signal for phagocytes (Segawa and Nagata, 2015; Zhang et al., 2018); (iii) cell shrinkage (apoptotic volume decrease, AVD) is followed by chromatin condensation and nuclear segmentation (Galluzzi et al., 2012, 2015, 2018); (iv) PM blebbing results in cell fragmentation into apoptotic bodies (Kroemer et al., 2005; Atkin-Smith and Poon, 2017) and their subsequent phagocytosis (Arandjelovic and Ravichandran, 2015).

The term “apoptotic-like PCD” (“AL-PCD”) was coined due to morphological and biochemical resemblance of stress-associated plant cell death to apoptosis, in particular AVD-like protoplast shrinkage, but also Ca^{2+}- and ATP-dependency, maintenance of PM integrity and involvement of caspase-like activity (Balk et al., 1999; Vacca et al., 2004; Hogg et al., 2011; Kacprzyk et al., 2017). Notably, “AL-PCD” is induced by an acute stress, e.g. a pulse heat shock (HS) at 55°C, a

temperature approximately 30°C above the physiologically relevant conditions that might in fact cause fatal damage to the cell leading to necrosis. Unlike apoptosis, necrosis is associated with a drop of cellular ATP content, does not depend on energy or caspases, and displays early PM permeabilization leading to the leakage of cellular contents into the extracellular environment (Ankarcrona et al., 1995; Majno and Joris, 1995).

To reconcile proposed features of "AL-PCD" with the apparent lack of the key components of the apoptotic machinery in plants, we systematically analysed reported "AL-PCD" hallmarks using appropriate controls for potential technical pitfalls. This revealed that while protoplast shrinkage superficially resembles AVD, it is neither dependent on ATP nor regulated by Ca^{2+}, but instead coincides with instant and irreversible loss of PM integrity. We also demonstrate the absence of key apoptotic events such as PM blebbing, nuclear segmentation, and formation of apoptotic bodies. In summary, we establish plant "AL-PCD" as an energy-independent process bearing only superficial resemblance to apoptosis, but perfectly matching definition of necrosis.

Results and discussion

HS-induced plant cell death is morphologically distinct from apoptosis

One of the earliest hallmarks of apoptosis is AVD (Bortner and Cidlowski, 2002, 2007), followed by blebbing of the PM, nuclear segmentation and finally fragmentation of the cell into apoptotic bodies that facilitates their uptake by phagocytes (Arandjelovic and Ravichandran, 2015). Death of plant cells caused by abiotic or biotic stress can be accompanied by the protoplast shrinkage, a phenomenon repeatedly exploited to support existence of plant apoptosis or "AL-PCD" (Kabbage et al., 2017; Dickman et al., 2017). However, as plants lack phagocytes, apoptotic body formation during plant cell death would unlikely serve a purpose (Bozhkov and Lam, 2011; Green and Fitzgerald, 2016). Nevertheless, there are studies claiming the occurrence of the PM blebbing and the formation of apoptotic bodies during plant PCD (for review see Dickman et al., 2017).

To examine AVD, PM blebbing, nuclear segmentation and cellular fragmentation in plants, we analysed morphology of Bright Yellow-2 tobacco cell cultures (BY-2) under HS conditions that induce "AL-PCD" (Balk et al., 1999; Kacprzyk et al., 2017). After a pulse HS at 55°C, the cell culture was stained with Sytox Orange (SO) nucleic acid dye to visualize cells with compromised PM integrity and with the styryl dye FM4-64 to visualize cell membranes (**Fig. 1, Supplementary Video S1**).

SO-negative cells lacked any apparent AVD or PM blebbing (**Fig. 1A, B)**. On the contrary, the SO-positive cells exhibited protoplast shrinkage and atypical vesicle-like structures at the inner side of the PM (**Fig. 1A, B)**. The cells became SO-positive already within 10 min of the HS indicating rapid PM permeabilization. The PM and shrunken protoplast were imaged at 15 min, 1, 2, 4, 6, 24, 48, and 72 h after the pulse HS (data not shown). Nevertheless, we failed to detect PM blebbing or protoplast fragmentation into discrete bodies at any time point. Furthermore, although we did observe moderate nuclear condensation upon HS, it was not followed by segmentation of the organelle (**Fig. 1C, D**). In summary, the gross morphological changes of cells undergoing "AL-PCD" do not resemble apoptosis.

PM integrity is irreversibly compromised during or shortly after pulse HS

Intact PM is a pivotal hallmark of apoptosis (Kroemer et al., 2005). However, SO staining suggested permeabilization of PM in most BY-2 cells already within 10 min of the HS. To investigate dynamics of the PM permeabilization, we analysed cellular content leakage after two types of HS: 55°C or 85°C, which were reported to induce "AL-PCD" or necrosis, respectively (McCabe et al., 1997; Reape and McCabe, 2013). The leakage of cellular content was assessed using a fluorescein diacetate (FDA)-based fluorochromatic assay (Rotman and Papermaster, 1966). In brief, the non-fluorescent FDA molecules can passively diffuse into the living cells where their acetate groups are cleaved off by esterases. The resulting fluorescein molecules have poor membrane permeability and are retained in cells with an intact PM, but are released into extracellular space upon PM permeabilization.

We imaged BY-2 cells loaded with FDA prior to the pulse HS at 55°C or 85°C (**Fig. 2A**). Both types of HS caused rapid (within 10 min) leakage of the dye into the extracellular space (**Fig. 2A**). We measured the amount of fluorescein accumulated in the extracellular space immediately after the HS and found that the rate of cellular content leakage in HS-treated cells is comparable to that occurring after freeze-thaw of cells in liquid nitrogen (**Fig. 2B**).

To determine whether PM permeabilization was transient or permanent, we added SO to the cell cultures either before or 1 h after HS. If PM permeabilization upon HS was transient, cultures stained after HS would show a significantly lower frequency of SO staining. However, SO staining before and after 55°C or 85°C HS showed no differences in the proportion of SO-positive cells (**Fig. 2C, D**), indicating that both treatments caused irreversible rapid permeabilization of PM typical for necrosis (Kroemer et al., 2005; Zong and Thompson, 2006; van Doorn et al., 2011).

The protoplast shrinkage during HS-induced cell death is ATP- and Ca^{2+}-independent

Dismantling of the apoptotic cells is ATP-dependent (Tsujimoto, 1997; Zamaraeva et al., 2005). Yet, loss of the PM integrity would lead to rapid depletion of intracellular ATP, rendering all energy-dependent processes defunct. To examine whether the HS-induced cell death requires ATP, we first imaged mitochondria after 55°C and 85°C HS. Within 4 min after HS, under both temperatures, mitochondrial dye MitoTracker localized to aberrant structures similar to those observed after treatment with mitochondrial uncoupler and ATP synthesis inhibitor, carbonyl

cyanide m-chlorophenylhydrazone (CCCP) (Perry et al., 2011), indicating disruption of mitochondrial membrane potential (MMP; **Fig. 3A**). Furthermore, intracellular ATP content dropped dramatically after both HS treatments (**Fig. 3B**), most probably due to dissipation of the MMP and leakage of cytoplasmic content through the permeabilized PM.

In addition to ATP depletion, PM permeabilization would also cause entry of Ca^{2+} into the cells, potentially followed by its accumulation in mitochondria. MMP-driven accumulation of Ca^{2+} can trigger mitochondrial permeability transition (MPT) due to the opening of a nonspecific pore (MPTP) in the inner mitochondrial membrane (Hunter and Haworth, 1979). Opening of MPTP leads to a collapse of the MMP, thereby causing arrest in ATP synthesis, and production of reactive oxygen species leading to necrotic cell death (Kristián and Siesjö, 1998). Although HS-induced plant cell death was previously suggested to be a Ca^{2+}-dependent process (Kacprzyk et al., 2017), those experiments lacked controls for mitochondrial phenotype, respiration, or ATP production.

To test whether MPT plays a role in the observed mitochondrial phenotype, experiments were performed in the presence of cyclosporin A (CsA), an inhibitor of MPTP opening, or the Ca^{2+} chelator EGTA. Neither CsA nor EGTA could alleviate the mitochondrial phenotype in cells subjected to the HS (**Fig. 3C, D**), indicating that mitochondrial malfunction was caused by the direct loss of the mitochondrial membrane integrity during the HS, independently on PM permeabilization.

Next, we examined the importance of intracellular ATP for the AVD-like protoplast shrinkage. We found that pre-treatment of the cell cultures with CCCP prior to HS had no effect on the protoplast shrinkage (**Figs. S1A, B**), demonstrating that the protoplast shrinkage does not require ATP. Time-resolved quantitative analysis of cell death (frequency of SO-positive cells) and protoplast shrinkage upon HS of cells with normal or uncoupled mitochondria revealed that both parameters were independent of the mitochondrial bioenergetic function (**Fig. 3E, F**). Pre-treatment with CsA or EGTA prior to HS did not alleviate the cell death rate either **(Fig. 3G, H**, **Fig. S1C, D**).

The discrepancies between our work and the previous studies could be caused by technical issues, i.e. precision of the temperature measurement during HS. To examine this possibility, we performed HS at 40, 45 and 50°C. Although cell viability was inversely proportional to the temperature, the morphology of dead cells in all cases was identical to that observed at 55°C, and the rate of cell death did not depend on mitochondrial activity (**Fig. S1E-H**).

A recent study by Distéfano et al., (2017) proposed that HS at 55°C causes ferroptosis in *Arabidopsis thaliana* root hair cells. Although mitochondrial dysfunction is known to suppress ferroptosis in animal cells (Gao et al., 2019) and, as shown above, HS-induced plant cell death is mitochondria-independent, we still examined whether "AL-PCD" could be classified as a ferroptosis. For this, BY-2 cells were treated with a ferroptosis inhibitor, ferrostatin-1 (Fer-1), prior to HS at 55°C and cell death rate was measured during 24 h after the stress. Treatment with Fer-1 did not alleviate the cell death (**Fig. 4A, B;** data is shown for the first 12 h after HS). Furthermore, two independent experiments replicating conditions that were reported to induce ferroptosis in *Arabidopsis* root hair cells did not confirm such type of cell death (**Fig. 4C)**. Taken together, our results reject the notion that HS-induced "AL-PCD" is a programmed process. On the contrary, they demonstrate that HS triggers rapid destruction of cellular components and passive decay of plant cells, i.e. necrotic cell death.

Necrotic deaths caused by 55°C or 85°C display different cell morphologies due to a fixating effect of higher temperature

The lack of protoplast shrinkage during cell death induced by 85°C was used to classify it as necrosis (McCabe et al., 1997; Reape and McCabe, 2013). However, both 55°C and 85°C HS trigger instant and irreversible permeabilization of the PM, MMP dissipation, and drop in intracellular ATP content, i.e. hallmark features of necrosis. Plausibly, morphological differences between necrotic cell deaths triggered by 55°C and 85°C could be explained by rapid protein denaturation occurring at 85°C that would crosslink cellular components. Such "fixation" would prevent protoplast shrinkage. Consistent with this suggestion, high-temperature cell fixation protocols have been used as an alternative to chemical fixation (Login and Dvorak, 1988).

To test whether 85°C HS acts as a fixative, we induced protoplast retraction from the cell wall by exposing stressed cell cultures to hypertonic conditions at 185 mM D-mannitol (**Fig. 5**). The high osmotic pressure would induce dehydration and protoplast shrinkage in the non-fixed cells. As expected, the living cells treated with D-mannitol underwent typical plasmolysis manifested by reversible protoplast detachment from the cell wall. Cells exposed to 55°C displayed irreversible protoplast shrinkage phenotype both with and without D-mannitol treatment. However, although cells treated at 85°C HS exhibited visible signs of dehydration in the hypertonic solution, protoplasts of virtually all cells remained attached to the cell wall. These data provide compelling evidence that the fixing effect of 85°C HS prevents protoplast shrinkage. Thus, morphological differences between 55°C and 85°C HS-induced cell deaths do not reflect differences in the cell-death execution mechanism.

Conclusions

Research on plant cell death suffers from superficial extrapolation of the rich knowledge about various types of animal cell death, and in particular *bona fide* apoptosis that is especially appealing due to immense track record of ground-breaking discoveries. Results of our current work schematically summarized in **Fig. 6** indicate that morphological and molecular characteristics of plant HS-induced cell death termed in the literature "AL-PCD" *de facto* fit the definition of necrosis. The set of assays described here can be easily implemented to various plant model systems used for the investigation of cell death with "apoptotic-like" features (e.g., Ryerson and Heath, 1996; Navarre and Wolpert, 1999; Houot et al., 2001; Behboodi and Samadi, 2004; Tada et al., 2005; Lytvyn et al., 2010; Rybaczek et al., 2015; Nyalugwe et al., 2016; Ambastha et al., 2017; Żabka et al., 2017; Araniti et al., 2018; Malerba and Cerana, 2018; Ghasemi et al., 2020). This will hopefully bring the question about existence of plant apoptosis to rest before long. Our study highlights the need for critical classification of plant cell death modalities (van Doorn et al., 2011) which is crucial for understanding the evolution of eukaryotic cell death machinery.

Methods

Plant material and growth conditions

BY-2 cell cultures (Nagata et al., 1992) were grown at 25°C (unless stated otherwise), 120 rpm, in the darkness. Cells were subcultured every 7 days to the standard Murashige and Skoog (MS)

medium supplemented with vitamins (M0222, Duchefa), 1.875 mM KH_2PO_4, 0.2 mg/L 2,4-D, and 3% (w/v) sucrose; pH 5.6.

For growing *Arabidopsis thaliana* seedlings, Col-0 seeds were sterilized for 30 min using a 2.7 g/L sodium hypochlorite solution (Klorin, Colgate Palmolive) with 0.05% (v/v) Tween 20. The seeds were then rinsed three times with filter-sterilized Milli-Q water prior to being plated on solidified medium. The MS medium was brought to pH 5.8 with 1M KOH prior to autoclaving and contained half-strength MS salts and vitamins (M0222, Duchefa), 1% (w/v) sucrose, 10 mM MES and 0.8% (w/v) plant agar (P1001, Duchefa). The plates were incubated vertically with cycles of 16 h of 150 µE m^{-2} s^{-1} light at 22°C/8 h of dark at 20°C.

Fluorescein leakage assay (fluorochromatic assay)

Cells were stained with 4 µg/mL FDA (Merck, F7378) in the culture medium for 10 min at room temperature. Half a mL aliquots of the stained cell culture were then transferred into 2 mL Eppendorf tubes using a cut 1-mL tip to avoid mechanical damage of the cells. Each tube was treated as a biological replicate. At least three replicates were used for each condition in each experiment.

The tubes were exposed to four conditions: (i) left on the bench at room temperature; incubated for 10 min at (ii) 55°C or (iii) 85°C in a preheated thermoblock (wells were filled with water for better thermoconductivity); (iv) snap frozen in liquid nitrogen. After treatments, cultures were let to cool down or thaw for 5 min at room temperature and then either mounted on a sample glass to be imaged using CLSM or processed further for quantitative assay.

For quantitative fluorescein leakage assay cells were pelleted on nylon meshes with 50 µm pores. Supernatants were collected entirely with a pipette, 150 µL of each supernatant were transferred to the empty wells of a 96-well flat bottom plate (Sarstedt). Cells on the mesh were then washed off the meshes into wells of the same plate using 150 µL of fresh BY-2 media. Fluorescence was measured in the FLUOstar Omega Microplate Reader (BMG LABTECH) using 485 nm excitation/520 nm emission filters (gain 800, 20 flashes/well). Importantly, the measurement had to be performed within 20 min after treatment to avoid passive diffusion of fluorescein into

extracellular space in the control samples. Leaked fluorescein intensity was calculated for each sample as a percentage of total fluorescence intensity detected in the cells and supernatant. A one-way ANOVA with a Dunnet's test was performed using JMP 10, and the graph was built in Origin2019.

Sytox Orange and FM4-64 staining

One-mL aliquots of 4-5-day old BY-2 cell culture were transferred to 1.5 mL Eppendorf tubes using a cut 1 mL tip. The final concentrations of Sytox Orange (SO; ThermoFisher, S11368) and FM4-64 (ThermoFisher, T3166) in cell culture were 1 µM and 0.5 µM, respectively. Five different treatments were applied to the cell cultures: (i) As a control, stained cell culture was incubated on the lab bench for 30 min. (ii) Stained cell culture was incubated in a preheated thermoblock at 55°C for a 10-min HS. (iii) Cell culture was subjected to a 55°C HS for 10 min, and stains were added after additional 30 min at room temperature. (iv) Stained cell culture was incubated in a preheated thermoblock at 85°C for a 10-min HS. (v) Cell culture was subjected to a 85°C HS for 10 min, and stains were added after additional 30 min at room temperature. Cells were mounted on a microscope slide and imaged by CLSM 30 min after staining. More than one hundred cells were counted for each treatment to ensure robustness of the results. Note that there is some degree of crosstalk in the fluorescence emission profiles of the SO and FM4-64 stains, which was most prominent following 85°C HS; however this crosstalk had no influence on the results of our experiments.

Importantly, following a 10-min pulse HS at 55°C, we observed that there are two distinct SO staining patterns: (i) cells with collapsed protoplasts that have intense staining (arrow, **Supplementary Fig. S2A**) and (ii) cells that have not collapsed with low intensity nuclear staining (arrowhead, **Supplementary Fig. S2A**). We found that the majority of cells were SO-positive within 10 min after the HS and that the proportion of cells with low intensity staining (i.e. those with only SO-positive nuclei) decreased over time as more cells collapsed and displayed intense SO staining (**Supplementary Fig. S2B)**.

Nuclear phenotyping

A transgenic BY-2 line expressing GFP fused to nuclear localization signal (NLS) under a double 35S promoter (2x35::Rluc-sGFP-NLS) was used to evaluate nuclear phenotype following HS. The transgenic culture was generated according to (Dauphinee et al., 2019). Treatments included: (i) No HS, (ii) 10-min pulse HS at 55°C (iii) 10-min pulse HS at 55°C with SO staining as stated above, which was used to validate results following HS (data not shown). Six hours following HS, z-stack acquisitions were captured with Zeiss LSM 800 as described in the *Confocal microscopy*. Quantification was performed using maximum intensity projections. The areas of nuclei were approximated using threshold segmentation of images with Fiji software (ImageJ version 1.52r). Three independent experiments were carried out.

MitoTracker Red Staining

BY-2 cells were stained with 100 µM MitoTracker Red (ThermoFisher, M7512) for 10 min at room temperature. Cells were mounted on a microscope slide and imaged using Zeiss LSM 780 as described in the *Confocal microscopy*.

EGTA and cyclosporin A treatments

Half a mL of a 4-5-day old BY-2 cell culture were transferred to 1.5 mL Eppendorf tubes. The cells were stained with Mitotracker Red (100 µM) and FDA (2 µg/mL) 10 min prior to treatment. Four different treatments (all at room temperature) were applied prior to 10-min HS at 55°C: (i) 10 mM EGTA (Merck, E3889), pH 8.0 for 10 min, (ii) 0.1% DMSO for 2 h, (iii) 15 µM cyclosporin A (CsA) for 2 h, and (iv) 10 mM EGTA (applied 10 min prior to HS) and 15 µM CsA (applied 2 h prior to HS). Treatment times were staggered and samples were scanned within 10 min following HS. Cells were mounted on a microscope slide and imaged using Zeiss LSM 800.

In order to assess the cell death rate following EGTA treatment, an additional experiment was carried out using BY-2 cells that were treated and then stained with SO and FM4-64 as described above. There were three biological replicates for each treatment group: (i) No HS - control (water), (ii) No HS – EGTA, (iii) 10-min 55°C HS – control, and (iv) 10-min 55°C HS - EGTA. After HS, 300 µL of each sample was transferred to a 24-well plate designed for fluorescent microscopy (µ-Plate 24, Ibidi 82406) and imaged using Zeiss LSM 780 as described in the *Confocal microscopy* section.

ATP content measurement

The assay was performed based on the previously published protocol (Minina et al., 2013). Half a mL aliquots of a 4-day-old BY-2 cell culture were transferred with a cut tip into 2 mL Eppendorf tubes. Six replicates were measured for each treatment in each experiment. The aliquoted cells were subjected to the treatments described in the *Fluorescein leakage* assay. Additionally, six aliquots were incubated with 48 µM carbonyl CCCP on the bench for 1 h. After treatment, cells were pelleted on a nylon mesh with 50 µm pores, rinsed with 3 mL of medium and washed off into new Eppendorf tubes with 600 µL of boiling buffer (100 mM Tris-HCl, 4 mM EDTA, pH 7.5, autoclaved and supplemented with phosphatase inhibitor cocktail 2 (Sigma-Aldrich, P5726)). During sample collection, the tubes were kept on ice. Samples were then boiled at 100°C for 10 min, and debris was spun down at 4°C, 10,000*g* for 20 min. The supernatants were transferred into new tubes and stored on ice.

For each sample, 83.5 µL of supernatant was transferred into wells of white Nunc plates in three technical replicates. The background signal was detected using FLUOstar Omega Microplate Reader (BMG LABTECH), with a lens filter taking ten measurements per well. 41.5 µL of freshly prepared reaction buffer (1.5 mM DTT, 100 µM Luciferin (Sigma L 6152), 5 µg/mL Luciferase from *Phontius pyralis* (Sigma L9506)) were pipetted into each well by the automated pump in a microplate reader. Luminescence was detected for each well after adding the reaction buffer and shaking the plate to ensure good mixing in the reaction volume. A serial dilution of ATP ranging from 1.8 10^{-2} M to 10^{-8} M was used to build a standard curve and calculate the amount of ATP in each sample. A one-way ANOVA with Dunnet's test was performed using JMP 10, and the graph was built in Origin 2019.

CCCP treatment

Half a mL of 4-5-day old BY-2 cell culture were transferred to 1.5 mL Eppendorf tubes using a cut 1 mL tip. The four treatment groups included: (i) 10-min treatment with 48 µM CCCP at room temperature followed by 55°C HS for 10 min, (ii) 0.1% DMSO (vehicle control) at room temperature for 10 min followed by 55° HS for 10 min, (iii) 10-min treatment with 48 µM CCCP and no HS, and (iv) 0.1% DMSO with no HS. The cultures were stained with 1 µM SO and then

transferred to a 24-well plate designed for fluorescent microscopy (µ-Plate 24, Ibidi 82406). Scanning of the wells was performed automatically using CLSM, 10 minutes after treatment and then every 2 h for 24 h. Three replicates were carried out per treatment group.

A HS gradient experiment was also carried out, comparing control (DMSO-) and CCCP-treated BY-2 cells. The cultures were stained and treated as per the CCCP experiment described above and then subjected to 10-min exposure to one of the following conditions: (i) no HS, (ii) 40°C HS, (iii) 45°C, (iv) 50°C, and (v) 55°C. The cultures were scanned after 6 h and 24 h using CLSM. Three technical replicates were carried out per group.

Osmotic stress assay

Two hundred µL of BY-2 cell culture were transferred into Eppendorf tubes. Cells were stained with FDA and exposed to HS as described in the *Fluorescein leakage assay*. 60 µL of 0.8 M D-Mannitol were added to each tube (final concentration 185 mM), cells were incubated at room temperature for 5 min and mounted on sample glass for CLSM imaging.

Ferroptosis assays

Three mL of 4-5-day old BY-2 cell culture were transferred to a 6-well plate using a cut 1 mL tip. Five different treatments were applied to the cell cultures for 16 h during which time they were returned to the incubator and grown as described above: (i) 0.1% DMSO (vehicle control), (ii) 1 µM Ferostatin-1 (Fer-1, Sigma SML0583), (iii) 10 µM Fer-1, (iv) 50 µM Fer-1 and (v) 100 µM Fer-1. After the 16-h treatments, 0.5 mL of culture from each well were transferred to 1.5 mL Eppendorf tubes using a cut 1 mL tip and separated into three treatments: (i) no HS, (ii) 55° HS for 10 min, or (iii) 85° HS for 10 min as described above. Following treatment, 10 µL of culture were transferred to 490 µL of fresh BY-2 media and stained with 1 µM SO and 0.5 µM FM4-64 in 24-well plates designed for fluorescent microscopy (µ-Plate 24, Ibidi 82406). Three technical replicates were carried out for each group and the wells were scanned automatically using CLSM at the following intervals: 10 min, 3, 6, 9, 12, 15, 18, 21 and 24 h. Three independent experiments were carried out.

The effect of Fer-1 was also tested on *Arabidopsis thaliana* seedlings which were grown as described above. Six-day old seedlings were gently transferred to 6-well plates containing 3 mL of liquid half-strength MS medium and given one of the following three treatments for 16 h: (i) 0.1% DMSO (vehicle control), (ii) 1 µM Fer-1, and (iii) 10 µM Fer-1. The treated medium was pipetted gently over the seedlings to ensure that roots were submerged in the liquid prior to being placed back into the growth cabinet overnight. The following morning, the seedlings were carefully transferred to 1.5 mL Eppendorf tubes containing the same treatment media from the 6-well plates before subjection to one of the following three treatments: (i) no HS, (ii) 55° HS for 10 min, or (iii) 85° HS for 10 min as described above. The seedlings were then stained with SO and FM4-64 as described above and placed back into the growth cabinet until scanning with CLSM at 3 h and 6 h post-HS. The early differentiation zone of the root was scanned for three seedlings per time point, and three independent experiments were carried out.

Confocal microscopy

Micrographs were acquired using either a LSM 800 or LSM 780 confocal laser scanning microscope (Carl Zeiss) with GaAsP detectors. Micrographs were taken with four different objectives: x10 (NA0.45), x20 (NA0.8), x40 (NA1.2, water immersion), and x63 (NA1.2, water immersion). For Fig. 1A-D and supplementary video S1, z-stack acquisition with sequential scanning was performed with a x63 objective. Nuclear phenotyping using the BY-2 transgenic line (Fig. 1E) was done with z-stack acquisitions using a x20 objective. Fluorescein was excited at 488 nm and emission was detected from 499 – 560 nm. MitoTracker red was excited at 561 nm and emission was detected from 582 – 754 nm. SO was excited at 561 nm and emission was detected from 410 – 605 nm. FM4-64 excitation was 506 nm, the emission was detected from 650 – 700 nm. Images were acquired using ZEN blue software (version 2.5, Carl Zeiss) or Zen black (version 2.3).

Acknowledgements

This project was supported by grants from Carl Tryggers Foundation (to EAM), MSCA IF (to EAM), the Swedish Research Councils VR (to PVB) and Formas (to AND and PVB), the Knut and Alice Wallenberg Foundation (to PVB), the Swedish Foundation for Strategic Research (to PVB), the Natural Sciences and Engineering Research Council (NSERC) of Canada (to AND) and

by the research programme “Crops for the Future” at the Swedish University of Agricultural Sciences. APS is grateful to August T. Larsson Guest Researcher Programme for supporting his visits to the Swedish University of Agricultural Sciences. VG was supported by the Russian Science Foundation (grant 19-14-00122).

Competing Interests statement

The authors declare no conflicts of interest.

References

Ambastha, V., Sopory, S.K., Tiwari, B.S., and Tripathy, B.C. (2017). Photo-modulation of programmed cell death in rice leaves triggered by salinity. Apoptosis **22**: 41–56.

Ameisen, J.C. (2002). On the origin, evolution, and nature of programmed cell death: a timeline of four billion years. Cell Death Differ. **9**: 367–393.

Ankarcrona, M., Dypbukt, J.M., Bonfoco, E., Zhivotovsky, B., Orrenius, S., Lipton, S.A., and Nicotera, P. (1995). Glutamate-induced neuronal death: a succession of necrosis or apoptosis depending on mitochondrial function. Neuron **15**: 961–973.

Arandjelovic, S. and Ravichandran, K.S. (2015). Phagocytosis of apoptotic cells in homeostasis. Nat. Immunol. **16**: 907–917.

Araniti, F., Costas-Gil, A., Cabeiras-Freijanes, L., Lupini, A., Sunseri, F., Reigosa, M.J., Abenavoli, M.R., and Sánchez-Moreiras, A.M. (2018). Rosmarinic acid induces programmed cell death in Arabidopsis seedlings through reactive oxygen species and mitochondrial dysfunction. PLoS One **13**: e0208802.

Atkin-Smith, G.K. and Poon, I.K.H. (2017). Disassembly of the Dying: Mechanisms and Functions. Trends Cell Biol. **27**: 151–162.

Balk, J., Leaver, C.J., and McCabe, P.F. (1999). Translocation of cytochrome c from the mitochondria to the cytosol occurs during heat-induced programmed cell death in cucumber plants. FEBS Lett. **463**: 151–154.

Behboodi, B.S. and Samadi, L. (2004). Detection of apoptotic bodies and oligonucleosomal

DNA fragments in cadmium-treated root apical cells of Allium cepa Linnaeus. Plant Sci. **167**: 411–416.

Bortner, C.D. and Cidlowski, J.A. (2002). Apoptotic volume decrease and the incredible shrinking cell. Cell Death Differ. **9**: 1307–1310.

Bortner, C.D. and Cidlowski, J.A. (2007). Cell shrinkage and monovalent cation fluxes: Role in apoptosis. Arch. Biochem. Biophys. **462**: 176–188.

Bozhkov, P. V and Lam, E. (2011). Green death: revealing programmed cell death in plants. Cell Death Differ. **18**: 1239–1240.

Coll, N.S., Epple, P., and Dangl, J.L. (2011). Programmed cell death in the plant immune system. Cell Death Differ. **18**: 1247–1256.

Daneva, A., Gao, Z., Van Durme, M., and Nowack, M.K. (2016). Functions and Regulation of Programmed Cell Death in Plant Development. Annu. Rev. Cell Dev. Biol. **32**: 441—468.

Dauphinee, A.N., Cardoso, C., Dalman, K., Ohlsson, J.A., Fick, S.B., Robert, S., Hicks, G.R., Bozhkov, P. V., and Minina, E.A. (2019). Chemical screening pipeline for identification of specific plant autophagy modulators. Plant Physiol. **181**: 855–866.

Dickman, M., Williams, B., Li, Y., Figueiredo, P., and Wolpert, T. (2017). Reassessing apoptosis in plants. Nat. plants **3**: 773–779.

Distéfano, A.M. et al. (2017). Heat stress induces ferroptosis-like cell death in plants. J. Cell Biol. **216**: 463–476.

Dixon, S.J. and Stockwell, B.R. (2019). The Hallmarks of Ferroptosis. Annu. Rev. Cancer Biol. **3**: 35–54.

van Doorn, W.G. et al. (2011). Morphological classification of plant cell deaths. Cell Death Differ. **18**: 1241–1246.

Drost, H.-G., Janitza, P., Grosse, I., and Quint, M. (2017). Cross-kingdom comparison of the developmental hourglass. Curr. Opin. Genet. Dev. **45**: 69–75.

Edlich, F. (2018). BCL-2 proteins and apoptosis: Recent insights and unknowns. Biochem. Biophys. Res. Commun. **500**: 26–34.

Galluzzi, L. et al. (2015). Essential versus accessory aspects of cell death: recommendations of the NCCD 2015. Cell Death Differ. **22**: 58–73.

Galluzzi, L. et al. (2012). Molecular definitions of cell death subroutines: recommendations of the Nomenclature Committee on Cell Death 2012. Cell Death Differ. **19**: 107–120.

Galluzzi, L. et al. (2018). Molecular mechanisms of cell death: recommendations of the Nomenclature Committee on Cell Death 2018. Cell Death Differ. **25**: 486–541.

Gao, M., Yi, J., Zhu, J., Minikes, A.M., Monian, P., Thompson, C.B., and Jiang, X. (2019). Role of Mitochondria in Ferroptosis. Mol. Cell **73**: 354-363.e3.

Ghasemi, R., Sharifi, R., and Ghaderian, S.M. (2020). Studying the roles of calcium and magnesium in cell death in the serpentine native plant Alyssum inflatum NYÁRÁDY through cell suspension culture technique. Plant Physiol. Biochem. PPB **151**: 362–368.

Green, D.R. and Fitzgerald, P. (2016). Just So Stories about the Evolution of Apoptosis. Curr. Biol. **26**: R620–R627.

Hengartner, M.O. (2000). The biochemistry of apoptosis. Nature **407**: 770–776.

Hogg, B. V, Kacprzyk, J., Molony, E.M., O'Reilly, C., Gallagher, T.F., Gallois, P., and McCabe, P.F. (2011). An in vivo root hair assay for determining rates of apoptotic-like programmed cell death in plants. Plant Methods **7**: 45.

Houot, V., Etienne, P., Petitot, A.S., Barbier, S., Blein, J.P., and Suty, L. (2001). Hydrogen peroxide induces programmed cell death features in cultured tobacco BY-2 cells, in a dose-dependent manner. J. Exp. Bot. **52**: 1721–1730.

Hunter, D.R. and Haworth, R.A. (1979). The Ca2+-induced membrane transition in mitochondria: I. The protective mechanisms. Arch. Biochem. Biophys. **195**: 453–459.

Huysmans, M., Lema A, S., Coll, N.S., and Nowack, M.K. (2017). Dying two deaths - programmed cell death regulation in development and disease. Curr. Opin. Plant Biol. **35**: 37—44.

Jacobson, M.D., Weil, M., and Raff, M.C. (1997). Programmed Cell Death in Animal Development. Cell **88**: 347–354.

Jorgensen, I., Rayamajhi, M., and Miao, E.A. (2017). Programmed cell death as a defence against infection. Nat. Rev. Immunol. **17**: 151–164.

Kabbage, M., Kessens, R., Bartholomay, L.C., and Williams, B. (2017). The Life and Death of a Plant Cell. Annu. Rev. Plant Biol. **68**: 375–404.

Kacprzyk, J., Brogan, N.P., Daly, C.T., Doyle, S.M., Diamond, M., Molony, E.M., and McCabe, P.F. (2017). The retraction of the protoplast during PCD is an active, and interruptible, calcium-flux driven process. Plant Sci. **260**: 50–59.

Kerr, J.F., Wyllie, A.H., and Currie, A.R. (1972). Apoptosis: a basic biological phenomenon with wide-ranging implications in tissue kinetics. Br. J. Cancer **26**: 239–257.

Kristián, T. and Siesjö, B.K. (1998). Calcium in Ischemic Cell Death. Stroke **29**: 705–718.

Kroemer, G. et al. (2005). Classification of cell death: recommendations of the Nomenclature Committee on Cell Death. Cell Death Differ. **12 Suppl 2**: 1463–1467.

Lacomme, C. and Santa Cruz, S. (1999). Bax-induced cell death in tobacco is similar to the hypersensitive response. Proc. Natl. Acad. Sci. U. S. A. **96**: 7956–7961.

Letai, A. (2017). Apoptosis and Cancer. Annu. Rev. Cancer Biol. **1**: 275–294.

Login, G.R. and Dvorak, A.M. (1988). Microwave fixation provides excellent preservation of tissue, cells and antigens for light and electron microscopy. Histochem. J. **20**: 373–387.

Lytvyn, D.I., Yemets, A.I., and Blume, Y.B. (2010). UV-B overexposure induces programmed cell death in a BY-2 tobacco cell line. Environ. Exp. Bot. **68**: 51–57.

Majno, G. and Joris, I. (1995). Apoptosis, oncosis, and necrosis. An overview of cell death. Am. J. Pathol. **146**: 3–15.

Malerba, M. and Cerana, R. (2018). Role of peroxynitrite in the responses induced by heat stress in tobacco BY-2 cultured cells. Protoplasma **255**: 1079–1087.

Martínez-Fábregas, J., Díaz-Moreno, I., González-Arzola, K., Janocha, S., Navarro, J.A., Hervás, M., Bernhardt, R., Díaz-Quintana, A., and La Rosa, M.Á. (2013). New Arabidopsis thaliana cytochrome c partners: a look into the elusive role of cytochrome c in programmed cell death in plants. Mol. Cell. Proteomics **12**: 3666–3676.

McCabe, P.F., Levine, A., Meijer, P.-J., Tapon, N.A., and Pennell, R.I. (1997). A programmed cell death pathway activated in carrot cells cultured at low cell density. Plant J. **12**: 267–280.

Miao, E.A., Leaf, I.A., Treuting, P.M., Mao, D.P., Dors, M., Sarkar, A., Warren, S.E., Wewers, M.D., and Aderem, A. (2010). Caspase-1-induced pyroptosis is an innate immune effector mechanism against intracellular bacteria. Nat. Immunol. **11**: 1136–1142.

Minina, E.A. et al. (2020). Classification and Nomenclature of Metacaspases and Paracaspases: No More Confusion with Caspases. Mol. Cell **77**: 927–929.

Minina, E.A., Filonova, L.H., Sanchez-Vera, V., Suarez, M.F., Daniel, G., and Bozhkov, P. V. (2013). Detection and Measurement of Necrosis in Plants. In K. McCall and C. Klein, eds (Humana Press: Totowa, NJ), pp. 229–248.

Mitsuhara, I., Malik, K.A., Miura, M., and Ohashi, Y. (1999). Animal cell-death suppressors Bcl-xL and Ced-9 inhibit cell death in tobacco plants. Curr. Biol. **9**: 775-S1.

Molnár, T., Mázló, A., Tslaf, V., Szöllősi, A.G., Emri, G., and Koncz, G. (2019). Current translational potential and underlying molecular mechanisms of necroptosis. Cell Death Dis. **10**: 860.

Murat, F., van de Peer, Y., and Salse, J. (2012). Decoding plant and animal genome plasticity from differential paleo-evolutionary patterns and processes. Genome Biol. Evol. **4**: 917–928.

Nagata, T., Nemoto, Y., and Hasezawa, S. (1992). Tobacco BY-2 Cell Line as the “HeLa” Cell in the Cell Biology of Higher Plants. In International review of cytology.A survey of cell biology : Volume 132, K.W. Jeon and M. Friedlander, eds, International Review of Cytology TS - CrossRef. (Elsevier: London), pp. 1–30.

Navarre, D.A. and Wolpert, T.J. (1999). Victorin induction of an apoptotic/senescence-like response in oats. Plant Cell **11**: 237–249.

Nyalugwe, E.P., Barbetti, M.J., Clode, P.L., and Jones, R.A.C. (2016). Programmed cell death pathways induced by early plant-virus infection are determined by isolate virulence and stage of infection. Plant Pathol. **65**: 1518–1528.

Perry, S.W., Norman, J.P., Barbieri, J., Brown, E.B., and Gelbard, H.A. (2011). Mitochondrial membrane potential probes and the proton gradient: a practical usage guide. Biotechniques **50**: 98–115.

Reape, T.J. and McCabe, P.F. (2013). Commentary: the cellular condensation of dying plant cells: programmed retraction or necrotic collapse? Plant Sci. **207**: 135–139.

Rotman, B. and Papermaster, B.W. (1966). Membrane properties of living mammalian cells as studied by enzymatic hydrolysis of fluorogenic esters. Proc. Natl. Acad. Sci. **55**: 134.

Rybaczek, D., Musiałek, M.W., and Balcerczyk, A. (2015). Caffeine-Induced Premature Chromosome Condensation Results in the Apoptosis-Like Programmed Cell Death in Root Meristems of Vicia faba. PLoS One **10**: e0142307.

Ryerson, D.E. and Heath, M.C. (1996). Cleavage of Nuclear DNA into Oligonucleosomal Fragments during Cell Death Induced by Fungal Infection or by Abiotic Treatments. Plant Cell **8**: 393–402.

Salvesen, G.S., Hempel, A., and Coll, N.S. (2016). Protease signaling in animal and plant-regulated cell death. FEBS J. **283**: 2577–2598.

Segawa, K. and Nagata, S. (2015). An Apoptotic "Eat Me" Signal: Phosphatidylserine Exposure. Trends Cell Biol. **25**: 639–650.

Sperandio, S., Belle, I., and Bredesen, D.E. (2000). An alternative, nonapoptotic form of programmed cell death. Proc. Natl. Acad. Sci. U. S. A. **97**: 14376–14381.

Suzanne, M. and Steller, H. (2013). Shaping organisms with apoptosis. Cell Death Differ. **20**: 669–675.

Tada, Y., Kusaka, K., Betsuyaku, S., Shinogi, T., Sakamoto, M., Ohura, Y., Hata, S., Mori, T., Tosa, Y., and Mayama, S. (2005). Victorin triggers programmed cell death and the defense response via interaction with a cell surface mediator. Plant Cell Physiol. **46**: 1787–1798.

Tsujimoto, Y. (1997). Apoptosis and necrosis: intracellular ATP level as a determinant for cell death modes. Cell Death Differ. **4**: 429–434.

Vacca, R.A., Pinto, M.C., Valenti, D., Passarella, S., Marra, E., and Gara, L. (2004). Production of reactive oxygen species, alteration of cytosolic ascorbate peroxidase, and impairment of mitochondrial metabolism are early events in heat shock-induced programmed cell death in tobacco Bright-Yellow 2 cells. Plant Physiol. **134**: 1100–1112.

Valandro, F., Menguer, P.K., Cabreira-Cagliari, C., Margis-Pinheiro, M., and Cagliari, A. (2020). Programmed cell death (PCD) control in plants: New insights from the Arabidopsis thaliana deathosome. Plant Sci. **299**: 110603.

Yu, X.-H., Perdue, T.D., Heimer, Y.M., and Jones, A.M. (2002). Mitochondrial involvement in tracheary element programmed cell death. Cell Death Differ. **9**: 189–198.

Żabka, A., Winnicki, K., Polit, J.T., and Maszewski, J. (2017). Sanguinarine-induced oxidative stress and apoptosis-like programmed cell death(AL-PCD) in root meristem cells of Allium cepa. Plant Physiol. Biochem. PPB **112**: 193—206.

Zamaraeva, M. V, Sabirov, R.Z., Maeno, E., Ando-Akatsuka, Y., Bessonova, S. V, and Okada, Y. (2005). Cells die with increased cytosolic ATP during apoptosis: a bioluminescence study with intracellular luciferase. Cell Death Differ. **12**: 1390–1397.

Zhang, Y., Chen, X., Gueydan, C., and Han, J. (2018). Plasma membrane changes during programmed cell deaths. Cell Res. **28**: 9–21.

Zong, W.-X. and Thompson, C.B. (2006). Necrotic death as a cell fate. Genes Dev. **20**: 1–15.

Figure Legends

Figure 1. Gross morphological changes in HS-treated plant cells do not match hallmarks of apoptosis.

A FM4-64 and Sytox Orange (SO) dyes were used to visualize all cells and cells with permeabilized plasma membrane (PM), respectively. Stained BY-2 cells were imaged under control conditions (No HS) or after a 10-min HS at 55°C. Scanning was performed within 1 h post-HS. The arrows indicate PM; note the PM (red dotted line) being tightly pressed to the cell wall (white dotted line) under control conditions and detached under stress conditions. **B** Higher magnification of the areas indicated with arrows in **A**. **C** BY-2 cells expressing GFP fused to nuclear localization signal (NLS) were subjected to the same treatments as in **A**. Images represent maximum intensity projections of z-stack scans acquired 6 h post-HS. **D** Quantification of nuclear area in samples shown in **C**. Data from three independent experiments, with ≥ 142 cells counted per treatment. Student's t-test, *$p < 0.005$. DIC, differential interference contrast microscopy. n, nucleus. IQR, interquartile range. Scale bars, 20 µm (**A, C**) or 5 µm (**B**).

Figure 2. Both 55°C and 85°C HS cause instant and irreversible PM permeabilization.

A Green fluorescence in the BY-2 cells loaded with FDA. Fluorescein leaks into extracellular space within 10 min after HS at either 55°C or 85°C. Arrows indicate shrunken protoplasts in 55°C HS-treated cells. **B** Similar fraction of fluorescein leaks out of cells after 10 min of 55°C, 85°C, or liquid nitrogen (N_2) treatment. **C** BY-2 cells stained with SO and FM4-64. To assess whether disruption of the PM integrity after pulse HS is transient or irreversible, SO staining was performed before HS or 1 h after HS. **D** Frequency of the SO-positive cells in the cultures shown in **C**. DIC, differential interference contrast microscopy. IQR, interquartile range. Scale bars in **A** and **C**, 50 µm. **B**, representative data from one out of three independent experiments. **D**, data from three independent experiments, with ≥ 115 cells counted per treatment. **B** and **D**, one-way ANOVA with Dunnet's test; *, $p<0.005$.

Figure 3. Protoplast shrinkage at 55°C HS is an ATP- and Ca^{2+} -independent process.

A Mitochondria in BY-2 cells stained with MitoTracker Red and imaged 10 min after 55°C or 85°C HS, or after treatment with 48 µM CCCP. Severely damaged mitochondria were observed

upon all three treatments. **B** Loss of intracellular ATP content upon HS. Snap freeze-thaw treatment in liquid nitrogen (N_2) and CCCP treatment were used as positive controls for completely disrupted and uncoupled mitochondria, respectively. The experiment was repeated twice, each time using four biological replicates per treatment. **C** MitoTracker Red staining of BY-2 cells exposed to 55°C in the presence or absence of 15 µM Cyclosporin A (CsA) reveals that inhibition of MPTP opening does not rescue mitochondria from severe damage and loss of membrane potential caused by HS. **D** MitoTracker Red localization in the cells pre-treated with 10 mM EGTA prior to the HS reveals that chelation of extracellular Ca^{2+} does not rescue mitochondrial phenotype. **E, F** Dynamics of cell death (% SO-positive cells; **E**) and protoplast shrinkage **(F)** in cells with normal and uncoupled (48 µM CCCP treatment) mitochondria. **G, H** Pre-treatment with 10 mM EGTA before HS does not affect dynamics of cell death (% SO-positive cells; **G**) and protoplast shrinkage **(H)**. Experiments shown in **E-H** were repeated three times, with ≥ 184 cells per treatment and time point. Each microscopy experiment was performed at least twice. Scale bars, 20 µm (**A**) or 50 µm (**C, D**). IQR, interquartile range. **B**, **E-H**, one-way ANOVA with Dunnet's test; *, $p<0.05$.

Figure 4. HS-induced cell death response is not ferroptosis.

A Sytox Orange (SO) and FM4-64 staining of BY-2 cultures demonstrates that pre-treatment with 1 µM Ferrostatin-1 (Fer-1) does not affect 55°C HS-induced cell death. **B** Quantification of cell death (% SO-positive cells) in the samples illustrated in **A**. The chart shows representative results of three independent experiments, each including ≥ 280 cells per treatment and time point. **C** Pre-treatment with 1 µM Fer-1 does not alleviate the HS-induced death of *Arabidopsis thaliana* root hair cells. Arrows indicate SO-positive nuclei. Three independent experiments demonstrated the same results. No quantification was performed in these experiments, since all cells were SO-positive. DIC, differential interference contrast microscopy. Scale bars, 40 µm

Figure 5. 85°C HS prevents protoplast shrinkage in necrotic cells by fixing cellular content

Cells stained with FDA were exposed to 55°C or 85°C and mounted in the normal growth medium or hypertonic medium supplemented with 185 mM D-mannitol. High osmotic pressure induced plasmolysis in the non-stressed cells (no HS, arrows). Protoplasts of the cells treated at 55°C or 85°C only showed signs of dehydration in the hypertonic medium and no additional changes. The

frequency of protoplast detachment in the samples treated with 85°C remained close to zero even under high osmotic pressure, indicating that cells were fixed by the high-temperature treatment. White dotted line, cell wall; red dotted line, plasma membrane. Scale bars, 50 µm.

Figure 6. HS-induced plant cell death is necrotic rather than apoptotic process.

Plasma membrane (PM) integrity is maintained during apoptosis to prevent spillage of toxic dying cell contents. However, plant cell undergoing the so called ”AL-PCD” exhibit early irreversible permeabilization of PM, a feature typical for uncontrolled cell decay, necrosis. Apoptosis is associated with step-wise massive re-organization of the cellular morphology (nuclear segmentation, PM blebbing, fragmentation into apoptotic bodies) and thus is an energy consuming process that relies on controlled release of cytochrome *c*, functional mitochondria and intracellular ATP. On the contrary, necrotic death is a passive lysis of the cellular contents associated with low intracellular ATP and decoupled mitochondria. Similarly to necrotic animal cells, plant cells undergoing “AL-PCD” have an extremely low intracellular ATP content and uncoupled mitochondria. While apoptotic cells condense and disassemble into apoptotic bodies that are engulfed by phagocytes, a necrotic cell typically undergoes swelling that is followed by a decrease of the cell volume and leakage of the dead cell contents. Presence of the rigid cell wall most probably does not permit necrosis-like swelling of plant cells during “AL-PCD”, while rupture of the vacuole coinciding with permeabilization of the PM would lead to rapid leakage of the cellular contents and thus decrease in volume. Such shrinkage has very little in common with AVD, as it is a passive process not associated with the formation of apoptotic bodies.

Supplementary Figure and Video Legends

Figure S1. HS-induced cell death is ATP- and Ca^{2+} -independent process.

A-D Morphology of FDA-stained cells under normal conditions (no HS) and after a 55°C HS. Protoplast shrinkage is denoted by arrows. Pre-treatment with 48 µM CCCP for 10 min **(B)**, 15 µM CsA for 2 h **(C**), or 10 mM EGTA for 10 min (**D**) did not alleviate protoplast shrinkage upon HS. Each treatment was repeated at least twice. **E, G** Sytox Orange (SO) staining of BY-2 cells heat-shocked for 10 min at 40, 45, or 50°C and imaged after 6 h (**E**) and 24 h (**G**). Pre-treatment with CCCP provided no protection against cell death and protoplast shrinkage at any of the tested

HS temperatures. **F, H** Quantification of cell death (% SO-positive cells) in the samples shown in **E** and **G,** respectively. DIC, differential interference contrast microscopy. IQR, interquartile range. Experiments shown in **F** and **H** were repeated three times, with ≥ 170 cells per treatment and time point. The data was subjected to one-way ANOVA with Bonferroni correction. Scale bars, 20 µm **(A-D)** or 100 µm **(E, G).**

Figure S2. Different SO staining intensities following 55°C HS.

A Different intensity of SO staining in BY-2 cells exposed to 55°C HS for 10 min. Cells with shrunken protoplast (arrow) are brightly stained with SO whereas cells with normal-looking protoplasts have low-intensity nuclear staining (arrowhead). DIC, differential interference contrast microscopy. Scale bars, 50 µm. **B** Quantification of SO-positive cells over time. Most cells are SO-positive within 10 min of HS (0 h) and the proportion of cells with low SO intensity (arrowhead, **A**) decreases over time as more cells collapse and show intense staining (arrow, **A**). The experiment comprises three technical replicates, each including ≥ 180 cells per treatment and time point.

Supplementary Video S1. Shrinkage of plant protoplast caused by 55°C HS is not followed by fragmentation into apoptotic bodies. 3D reconstructions (maximum intensity projections) of BY-2 cells stained with FM4-64 to visualize the PM. Scanning was performed within 1 h post-HS. The arrows indicate membrane structures, which were not observed in the non-stressed (no HS) cells. These structures are localized on the inner side of the PM and do not separate from the cell at the later stages of cell death. Scale bars, 20 µm.

Figure 1

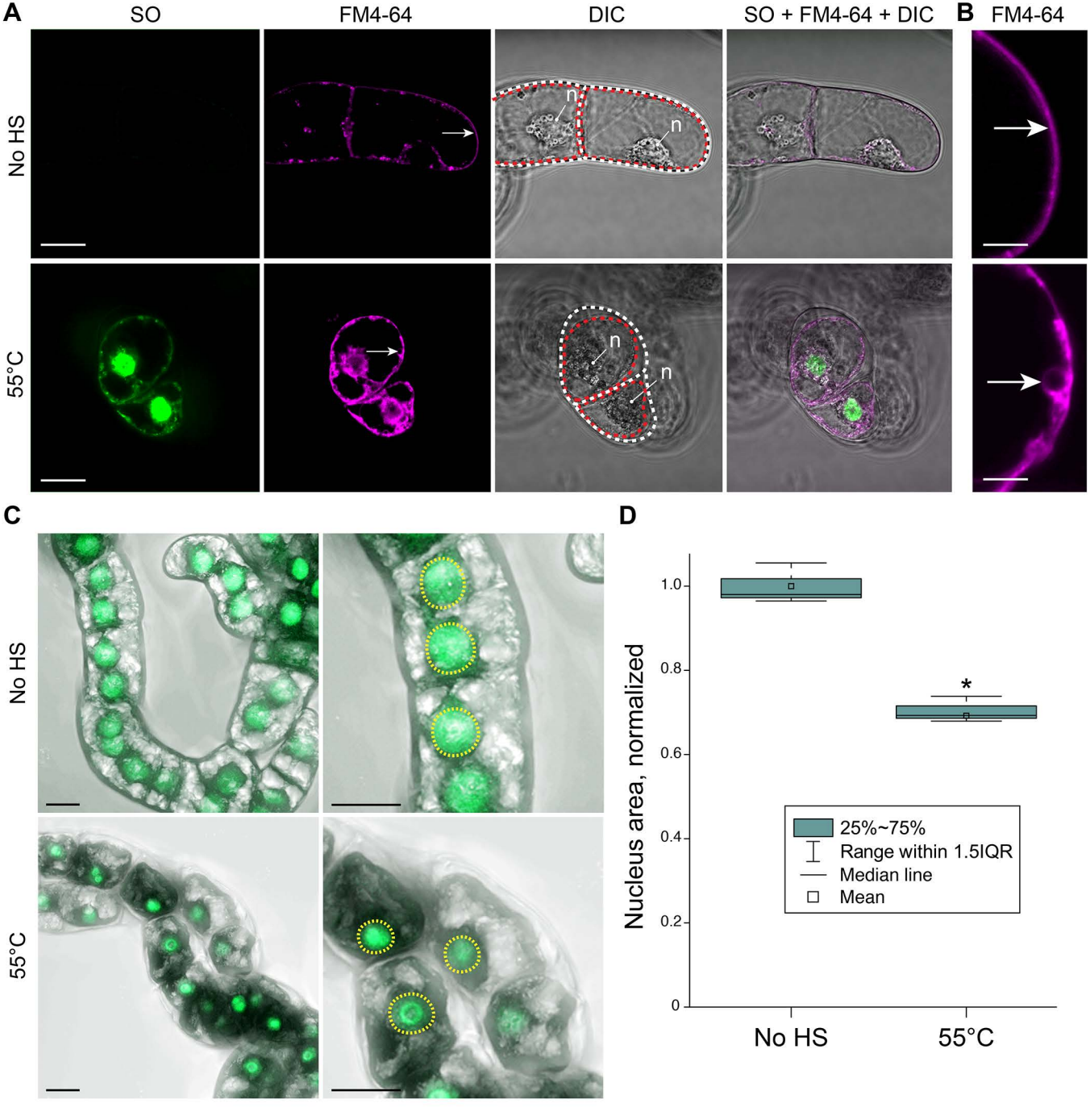
A
SO
FM4-64
DIC
SO + FM4-64 + DIC
B
FM4-64
No HS
55°C
n
C
D
Nucleus area, normalized
1.0
0.8
0.6
0.4
0.2
0
*
25%~75%
Range within 1.5IQR
Median line
Mean
No HS
55°C

Figure 2

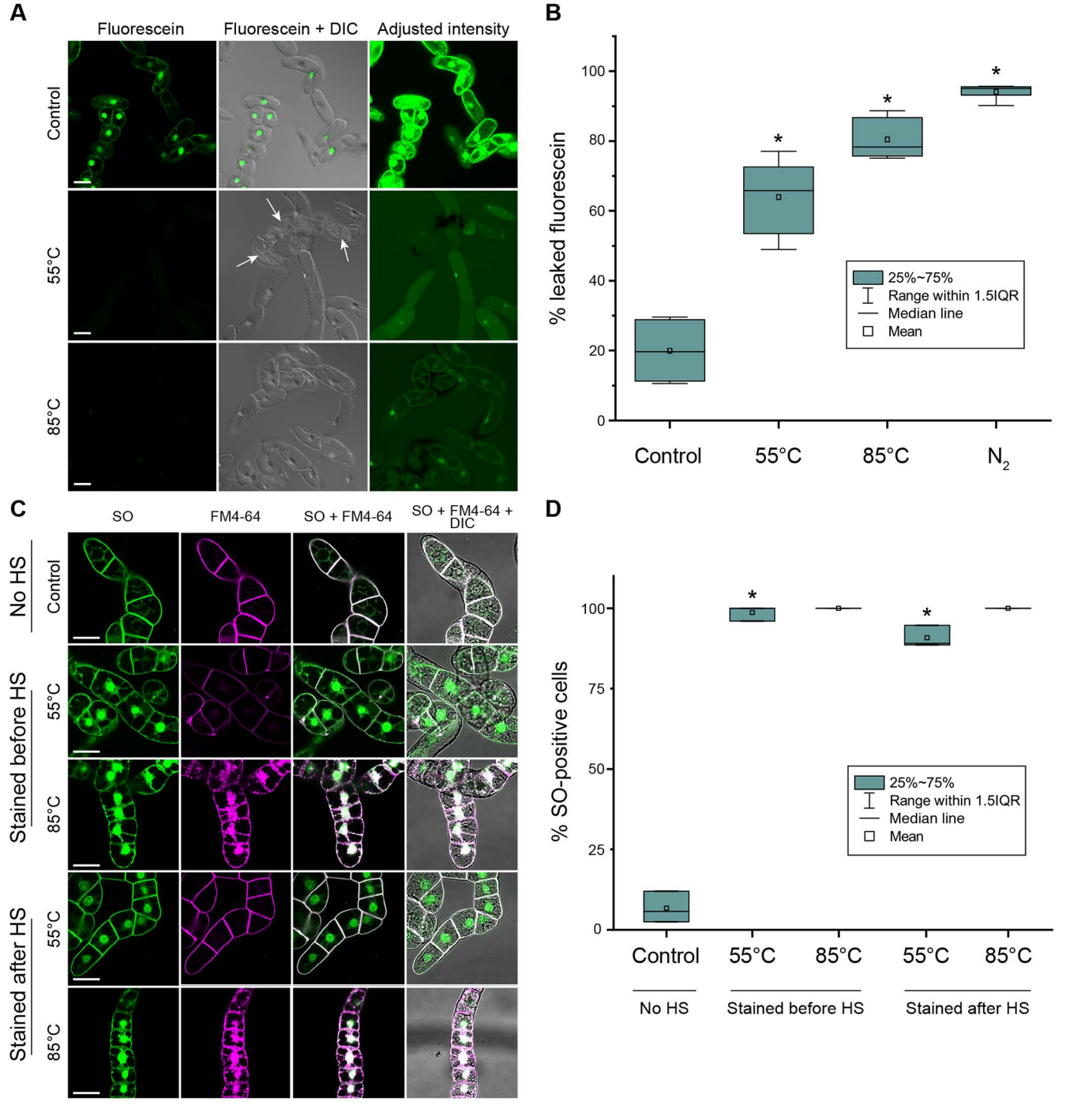
A
Fluorescein
Fluorescein + DIC
Adjusted intensity
Control
55°C
85°C
B
% leaked fluorescein
100
80
60
40
20
0
*
*
*
25%~75%
Range within 1.5IQR
Median line
Mean
Control
55°C
85°C
N2
C
SO
FM4-64
SO + FM4-64
SO + FM4-64 + DIC
No HS
Control
Stained before HS
55°C
85°C
Stained after HS
55°C
85°C
D
% SO-positive cells
100
75
50
25
0
*
*
25%~75%
Range within 1.5IQR
Median line
Mean
Control
55°C
85°C
55°C
85°C
No HS
Stained before HS
Stained after HS

Figure 3

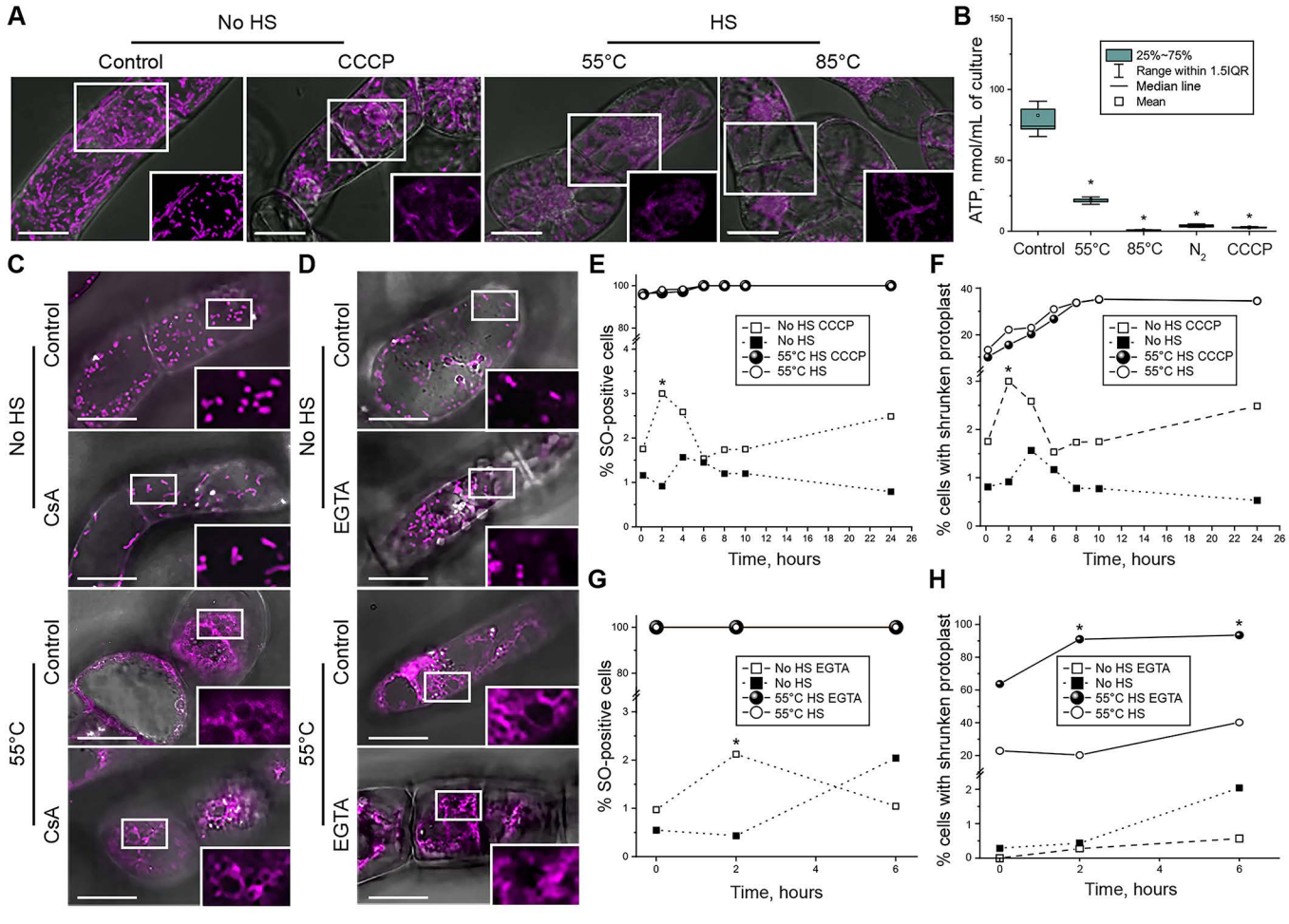
A
No HS
HS
Control
CCCP
55°C
85°C
B
ATP, nmol/mL of culture
25%~75%
Range within 1.5IQR
Median line
Mean
Control
55°C
85°C
N2
CCCP
C
No HS
Control
CsA
55°C
Control
CsA
D
No HS
Control
EGTA
55°C
Control
EGTA
E
% SO-positive cells
No HS CCCP
No HS
55°C HS CCCP
55°C HS
Time, hours
F
% cells with shrunken protoplast
No HS CCCP
No HS
55°C HS CCCP
55°C HS
Time, hours
G
% SO-positive cells
No HS EGTA
No HS
55°C HS EGTA
55°C HS
Time, hours
H
% cells with shrunken protoplast
No HS EGTA
No HS
55°C HS EGTA
55°C HS
Time, hours

Figure 4

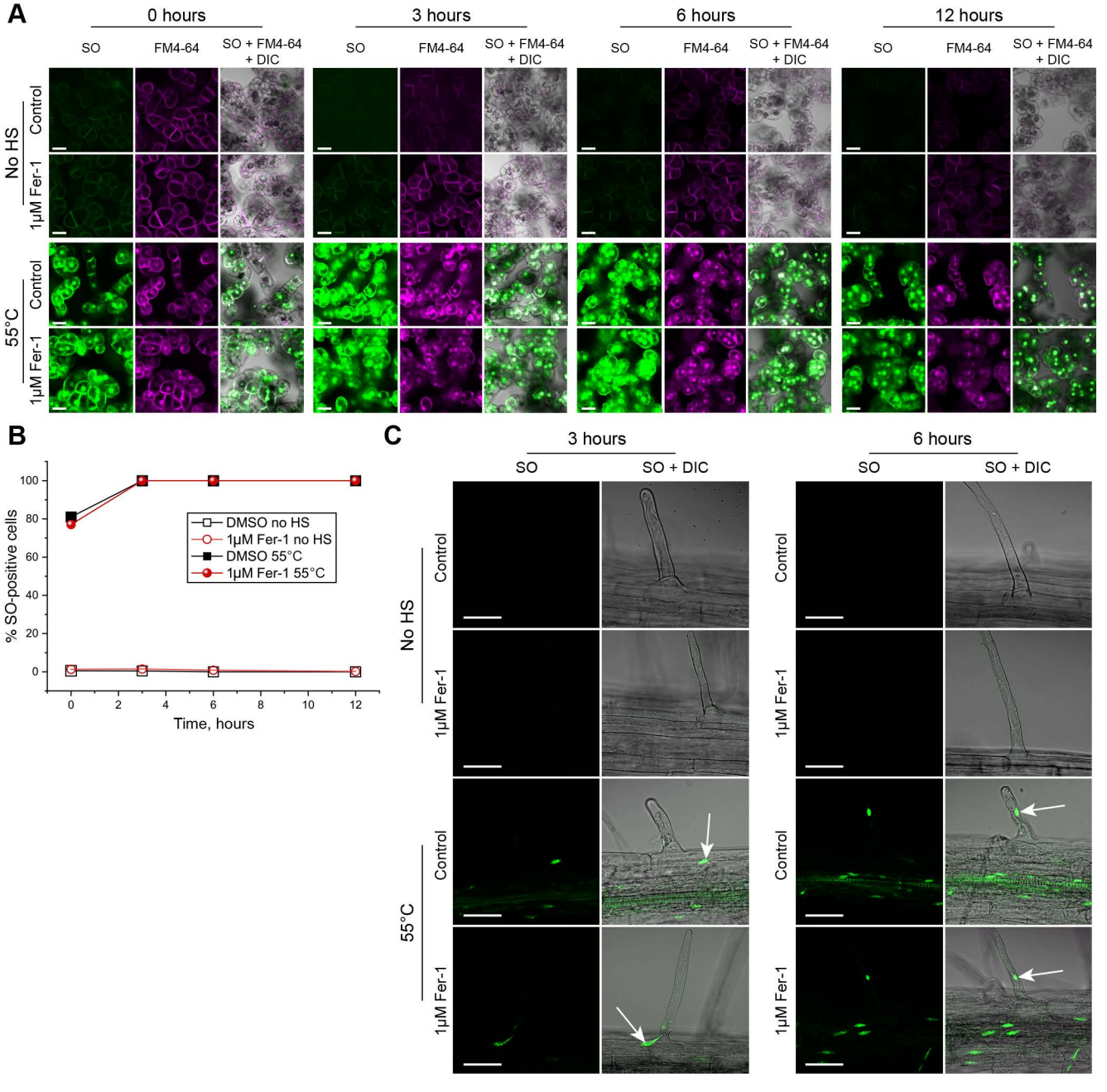
A
0 hours
3 hours
6 hours
12 hours
SO
FM4-64
SO + FM4-64 + DIC
No HS
Control
1μM Fer-1
55°C
B
% SO-positive cells
Time, hours
DMSO no HS
1μM Fer-1 no HS
DMSO 55°C
1μM Fer-1 55°C
C
3 hours
6 hours
SO
SO + DIC

Figure 5

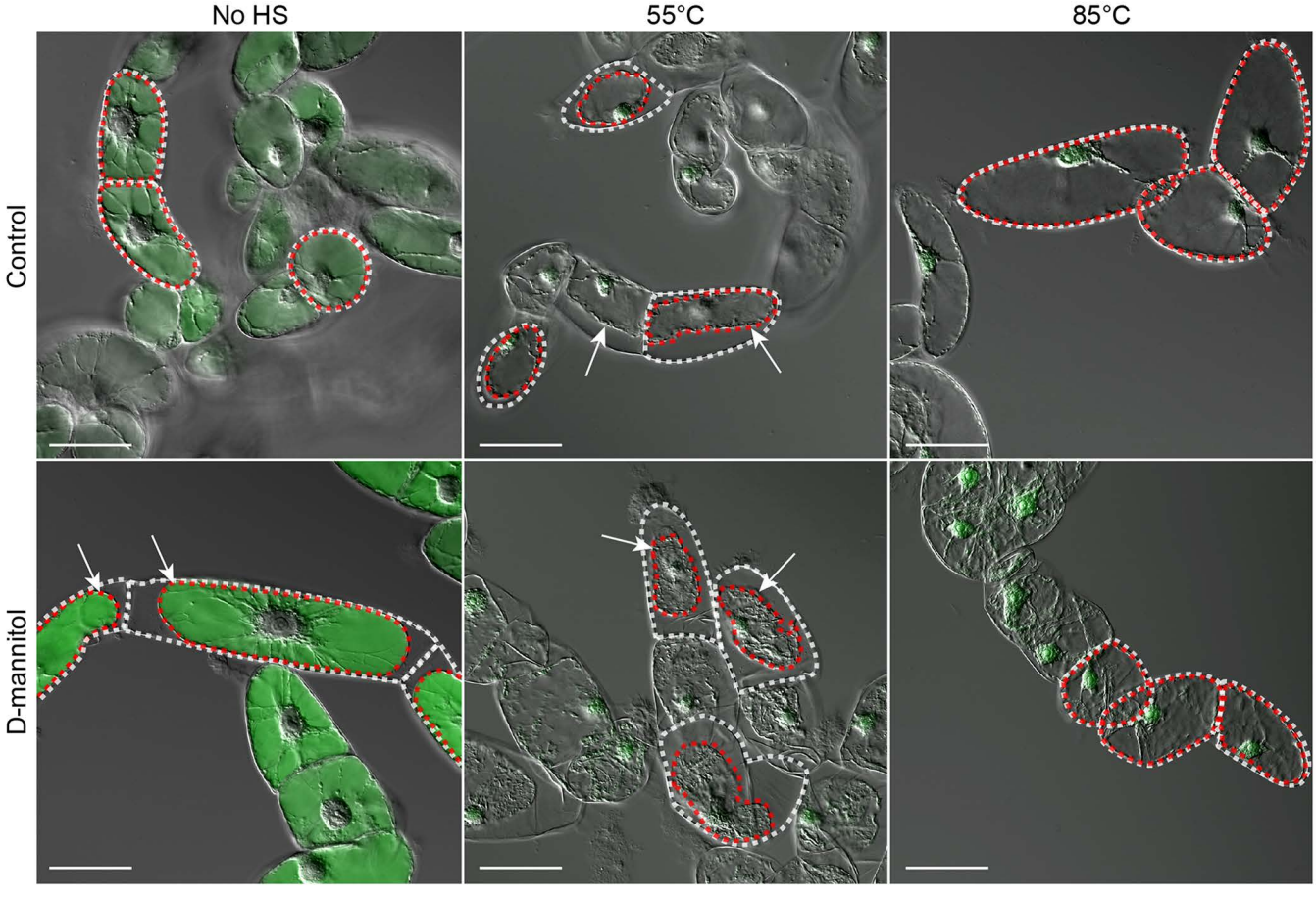

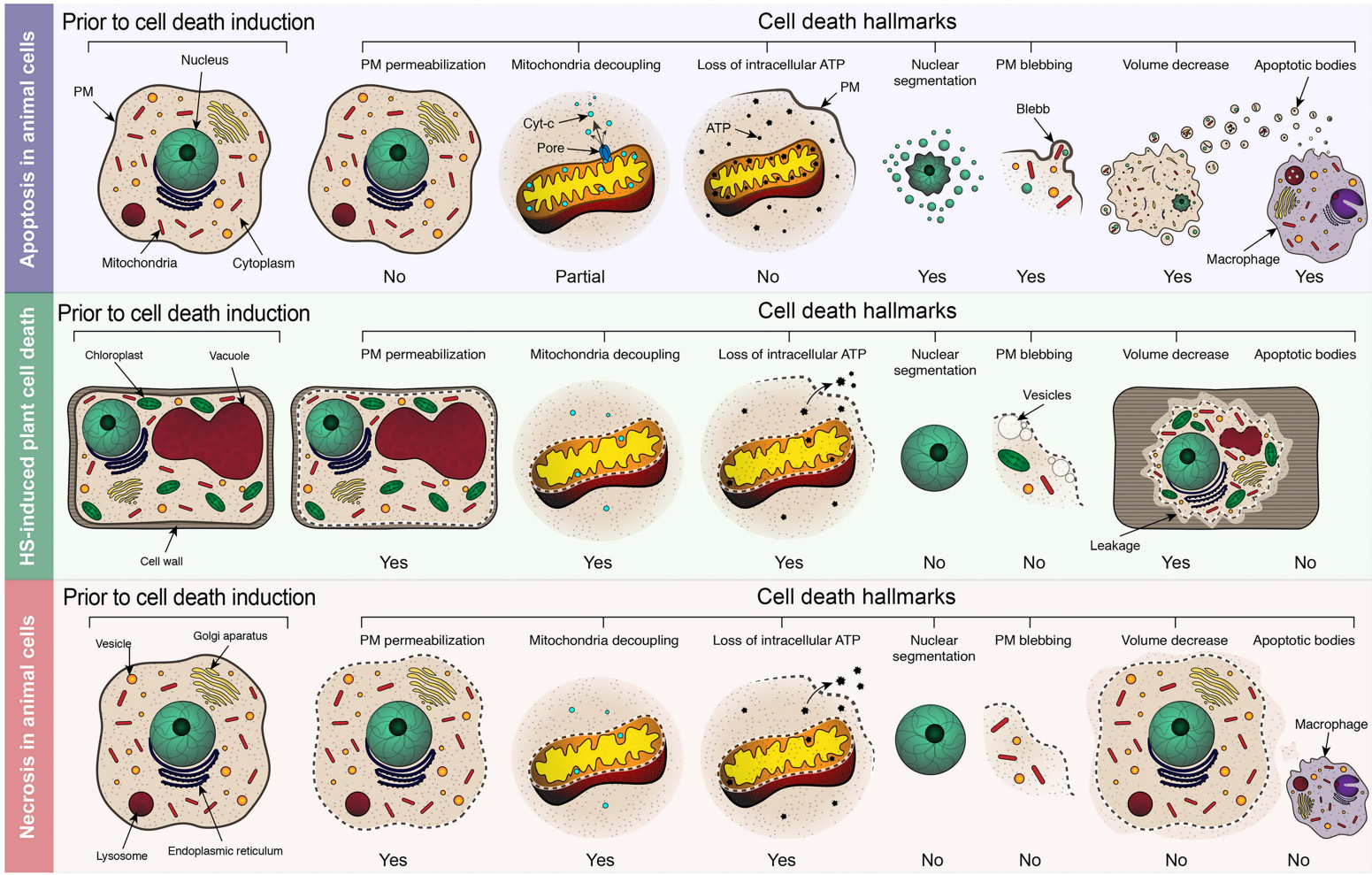
Apoptosis in animal cells
Prior to cell death induction
Nucleus
PM
Mitochondria
Cytoplasm
Cell death hallmarks
PM permeabilization
Mitochondria decoupling
Loss of intracellular ATP
Nuclear segmentation
PM blebbing
Volume decrease
Apoptotic bodies
Cyt-c
Pore
ATP
PM
Blebb
Macrophage
No
Partial
No
Yes
Yes
Yes
Yes
HS-induced plant cell death
Prior to cell death induction
Chloroplast
Vacuole
Cell wall
Cell death hallmarks
PM permeabilization
Mitochondria decoupling
Loss of intracellular ATP
Nuclear segmentation
PM blebbing
Volume decrease
Apoptotic bodies
Vesicles
Leakage
Yes
Yes
Yes
No
No
Yes
No
Necrosis in animal cells
Prior to cell death induction
Vesicle
Golgi aparatus
Lysosome
Endoplasmic reticulum
Cell death hallmarks
PM permeabilization
Mitochondria decoupling
Loss of intracellular ATP
Nuclear segmentation
PM blebbing
Volume decrease
Apoptotic bodies
Macrophage
Yes
Yes
Yes
No
No
No
No

Figure 6

Figure S1

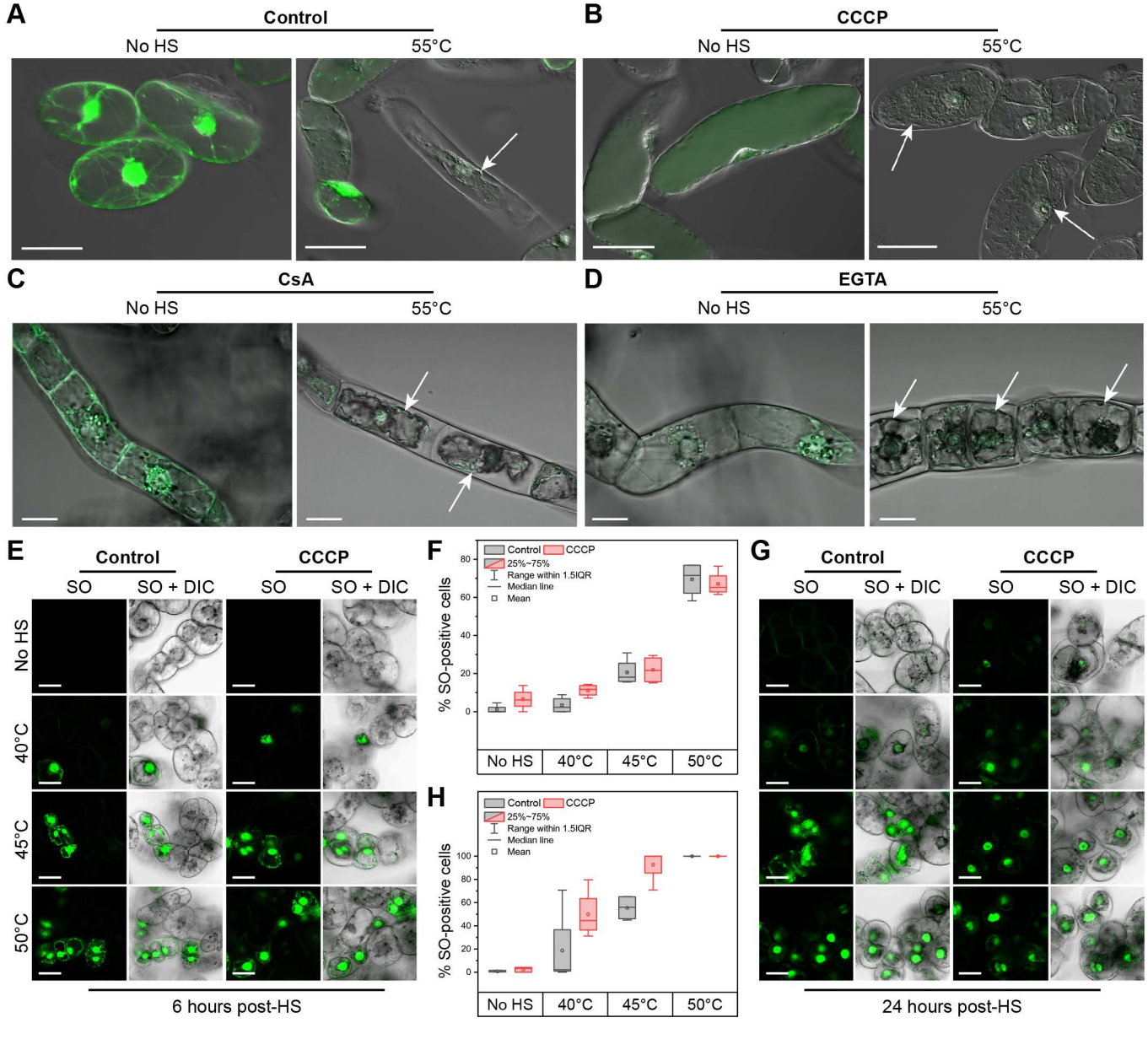
A
Control
No HS
55°C
B
CCCP
No HS
55°C
C
CsA
No HS
55°C
D
EGTA
No HS
55°C
E
Control
CCCP
SO
SO + DIC
SO
SO + DIC
No HS
40°C
45°C
50°C
6 hours post-HS
F
Control
CCCP
25%~75%
Range within 1.5IQR
Median line
Mean
% SO-positive cells
No HS
40°C
45°C
50°C
H
Control
CCCP
25%~75%
Range within 1.5IQR
Median line
Mean
% SO-positive cells
No HS
40°C
45°C
50°C
G
Control
CCCP
SO
SO + DIC
SO
SO + DIC
24 hours post-HS

Figure S2

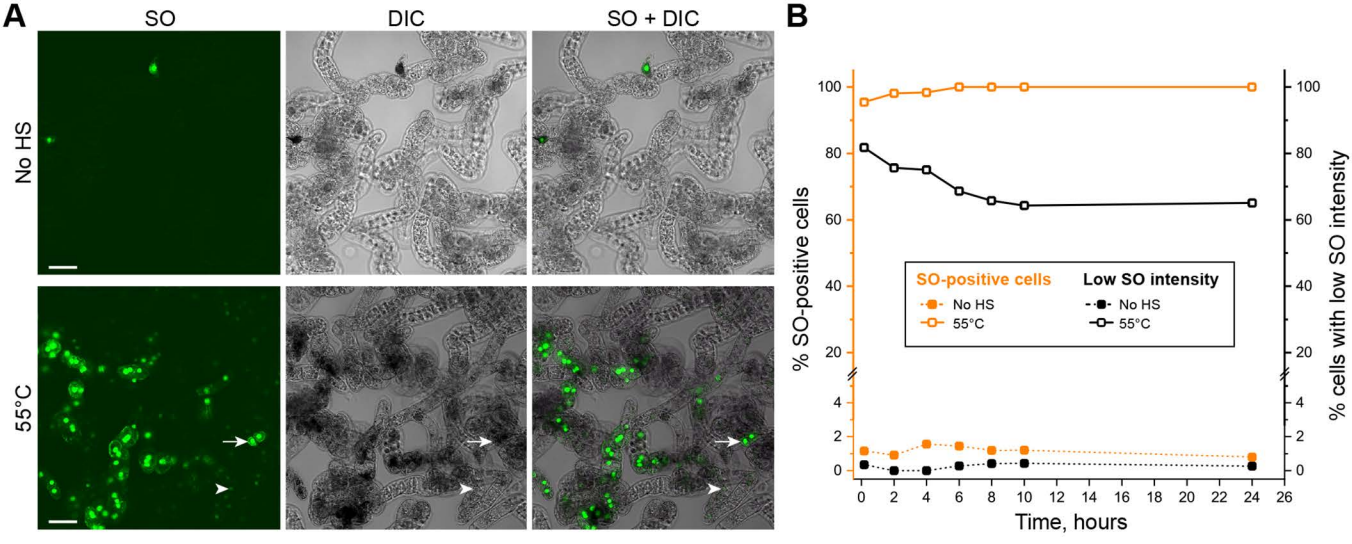
A
SO
DIC
SO + DIC
No HS
55°C
B
% SO-positive cells
% cells with low SO intensity
Time, hours
SO-positive cells
No HS
55°C
Low SO intensity
No HS
55°C